Comparison of RANS simulation and LES for the Prediction of Heat Transfer in a Highly Loaded Turbine Guide Vane

Nicolas Gourdain - Laurent Y.M. Gicquel

CERFACS, Computational Fluid Dynamics Team, CERFACS, Toulouse, France

Elena Collado

DT/MD/MO, TURBOMECA, Bordes, France

ABSTRACT

This paper proposes to investigate the flow in a highly loaded turbine guide vane with a particular interest for the estimation of wall heat fluxes. Two numerical approaches are assessed at different operating conditions: a steady-state method based on the Reynolds Averaged Navier-Stokes (RANS) equations and an unsteady approach based on the Large Eddy Simulation (LES). Results indicate that a steady flow simulation is able to predict wall heat transfers when boundary layers are either laminar or fully turbulent. However it fails to estimate the main flow features when a boundary layer transition phenomenon is observed. In this context, LES considerably improves the level of physical description (including boundary layer transition) and better estimates wall heat transfers. The paper also investigates the effect of Reynolds number and external turbulence intensity on the boundary layer transition mechanisms.

NOMENCLATURE

Latin	*Greek and symbols*
C Vane chord ($= 67.647\ mm$)	ρ Density
C_{wf} Wall friction coefficient (=2.$\tau_{wall}/(\rho u)_\infty$)	τ Shear stress ($= \nu\rho\frac{\partial u}{\partial y}$)
E Total energy	ν Kinematic viscosity
H Heat transfer coefficient	Θ Momentum thickness (=$\int_0^{+\infty} \frac{\rho u}{(\rho u)_\infty}(1-\frac{u}{u_\infty})dS$)
k Wave number	$._i$ / $._s$ Total (resp. static) value
L Length scale	$._{is}$ Isentropic value
M Mach number	$._0$ Inlet value
P Pressure	$._2$ Outlet value
q Heat flux	$._\infty$ Value outside the boundary layer
r Mixture gas constant ($= 287\ J.kg^{-1}.K^{-1}$)	$.^+$ Wall unit
Re Reynolds number	f' Fluctuating part
S Curvilinear abscissa	$\overline{f}$ Time averaged part
T Temperature	$\widetilde{f}$ Resolved flow field (Eq. 3)
Tu Turbulence level (=$\sqrt{u_x'^2}/\overline{u}$)	LES Large Eddy Simulation
u_i Velocity component in direction i	RANS Reynolds Averaged Navier-Stokes
	SEM Synthetic Eddy Method
	SGS Sub-Grid-Scale

INTRODUCTION

The transfer of thermal energy between a flow and a wall occurs in a lot of industrial applications (electronic circuit boards, gas turbine, etc.). The prediction of such wall heat transfers remains complex due to the interaction between different kinds of physics such as dynamic and thermal boundary layers, wall thermal properties, etc. In the context of gas turbine applications, the high pressure turbine experiences high temperature gradients at walls and its life duration directly relies on the capacity of designers to correctly estimate the wall heat transfer (Han et al. [2001]). Unfortunately, this result is difficult to predict in such a complex environment (high temperature, complex geometry including technological devices such as cooling holes, tip gap, etc.). Turbulence also plays a major role on heat transfer and a laminar to turbulent transition is often observed on the turbine blade walls. The main features of this complex phenomenon depend on many parameters such as the Reynolds number, turbulence intensity, wall roughness, shock, etc.

The physical understanding of these flows and the capability to efficiently predict heat transfer at the design stage is thus mandatory to improve the efficiency of gas turbines. In this regard a reliable Computational Fluid Dynamics (CFD) code represents a very attractive approach since it induces a relatively short response time in comparison to experimental campaigns. A large range of numerical methods is available in the literature to simulate near wall flows (Sagaut [2000]), from steady-state simulations where all the turbulent scales of the flow are modelled to full unsteady flow methods (the Direct Numerical Simulation -DNS- where all turbulent scales are solved). To complete the flow description when turbulence is modelled, criteria are necessary to predict the boundary layer transition (Abu-Ghannam and Shaw [1980], Mayle [1991], Johnson [1994], Menter et al. [2004]). There are also clear evidence in the literature that numerical methods that solve a part of the turbulent spectrum provide very promising results regarding the prediction of heat transfer (Duchaine et al. [2009], Zhong and Tucker [2005], Bhaskaran and Lele [2010]).

Based on this state-of-the-art, this paper proposes to compare the capability of RANS and LES methods to predict the wall heat transfer in a highly loaded turbine guide vane. The test case is a well documented configuration investigated by Arts et al. [1990] and extensively used for CFD validation (Liu [2007], Gehrer and Jericha [1999], Martelli et al. [2003], Boyle and Ameri [1997]). The first section of the paper presents the configuration and the second section details the numerical methods. Results are then compared with experiments for the estimation of the heat transfer coefficient in a third section. Various flow conditions are considered in terms of inlet turbulence intensity, Reynolds and Mach numbers. Finally, the physical mechanisms related to transition are discussed in the fourth section.

EXPERIMENTAL CONFIGURATION

The experimental facility is the isentropic light piston compression tube located at the Von Karman Institute (Fig. 1). The light weight piston is driven by the air of a high pressure tank in order to achieve the desired freestream gas conditions in terms of Mach and Reynolds numbers. More information about this facility is available in Consigny and Richards [1982]. The tested configuration is a 2D turbine vane cascade (the so-called LS 89 vane) largely described in Arts et al. [1990]. The vane is mounted in a linear cascade made of five profiles (only the central passage is investigated to ensure periodic flow conditions). The vane chord C is 67.647 mm with a pitch/chord ratio of 0.85. Experimental investigations were done to measure the velocity distribution by means of static pressure tappings and convective heat transfer by means of platinum thin films. Uncertainties were quantified for these measurements (pressure: $\pm 0.5\%$ and heat transfer coefficient: $\pm 5\%$). A large range of freestream conditions have been experimentally investigated but only three configurations are explored in this paper, as shown in Table 1 (test cases MUR129, MUR235 and MUR241). The considered Reynolds number (based on the chord and outlet velocity) ranges from 1.10^6 to 2.10^6 and

the inlet turbulence intensity Tu_0 ranges from 1% to 6%.

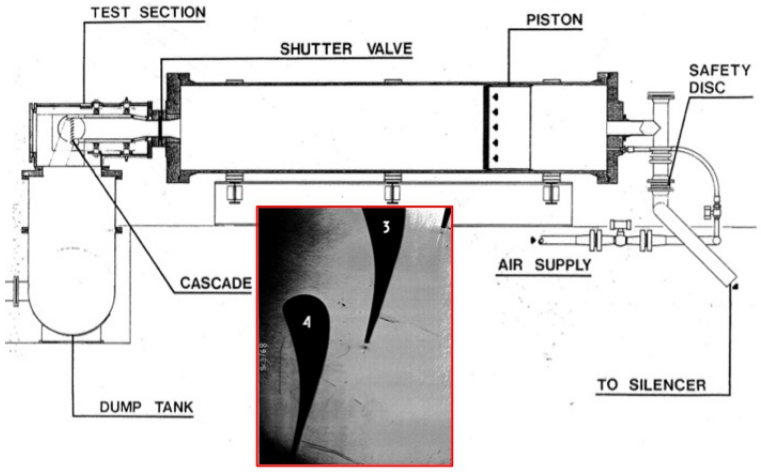

Figure 1: Experimental facility investigated by Arts et al. [1990]

The measurement technique to obtain wall heat fluxes is based on information provided by thin film gauges painted on the cascade central vane (made of glass ceramic) and an electrical analogy (Schultz and Jones [1973]). The thin films used for measurements are located in the the midspan region (where the time-averaged flow is 2D) and they cover 20% of the vane span (*i.e* 20 mm). The convective heat transfer coefficient H is then defined as the ratio between the wall heat flux and the difference between the total freestream and the local wall temperatures:

$$H = \frac{q_{wall}}{T_0 - T_{wall}} \tag{1}$$

Table 1: Test cases and details of the flow conditions

Test case	Re_2	$M_{is,2}$	$P_{i,0}$	$T_{s,wall}$	Tu_0
MUR129	$1.13\ 10^6$	0.840	$1.87\ 10^5\ Pa$	298 K	1.0%
MUR235	$1.15\ 10^6$	0.927	$1.85\ 10^5\ Pa$	301 K	6.0%
MUR241	$2.11\ 10^6$	1.089	$3.26\ 10^5\ Pa$	300 K	6.0%

TOOLS AND METHOD

Governing equations

The governing equations are the unsteady compressible Navier-Stokes equations that describe the conservation of mass, momentum and energy. In conservative form, it can be expressed in three-dimensional coordinates as:

$$\frac{dW}{dt} + divF = 0 \tag{2}$$

where W is the vector of primary variables, $F = (f - f_v, g - g_v, h - h_v)$ is the flux tensor; f, g, h are the inviscid fluxes and f_v, g_v, h_v are the viscous fluxes (including the potential contribution of models for turbulence through the value of ν_t). The fluid follows the ideal gas law $p = \rho\, r\, T$, where r is the

mixture gas constant. The fluid viscosity follows Sutherland's law and the heat flux follows Fourier's law.

The high Reynolds numbers related to the studied flow imply that all the flow scales can not be efficiently represented directly with current grid sizes (based on the typical Kolmogorov length scale, the magnitude order of the mesh size for a DNS in a turbulent channel should be around $Re^{\frac{9}{4}}$). Turbulence modelling is thus necessary to represent the cascade of energy and different formalisms exist over a wide range of applications, including flows at high Reynolds numbers. The most common approach for complex configurations is still the Reynolds-Averaged Navier Stokes methods (RANS) that propose to model the effect of all the turbulent scales on the mean flow. In this case, the boundary layer transition can be estimated by means of transition criteria (Abu-Ghannam and Shaw [1980], Mayle [1991], Johnson [1994], Menter et al. [2004]). This method has been applied to turbine flows with a moderate success (Martelli et al. [2003], Liu [2007], Boyle and Ameri [1997]): the criteria are effective to match the experiments (if the solution is known) but they usually suffer from a lack of universality (*i.e.* there are not easy to use in complex geometries and some physical phenomena are not taken into account). A promising method is the Large-Eddy Simulation (LES) that introduces a separation between the resolved (large) turbulent scales and the modelled (small) scales (Sagaut [2000], Pope [2000], Poinsot and Veynante [2005]). This separation of scales is obtained by filtering out the small flow scales that can not be properly represented by the mesh, their effects on the filtered field being modelled by the so-called Sub-Grid-Scale (SGS) model. LES involves the spatial Favre filtering operation that reduces for spatially, temporally invariant and localised filter functions to:

$$\widetilde{f(\mathbf{x},t)} = \frac{1}{\overline{\rho(\mathbf{x},t)}} \int_{-\infty}^{+\infty} \rho(\mathbf{x}',t)\, f(\mathbf{x}',t)\, G(\mathbf{x}'-\mathbf{x})\, d\mathbf{x}', \tag{3}$$

where G denotes the box filter function ($G = 1$ for spatial wavelengths $\lambda > \lambda_c$ else $G = 0$). The value of λ_c depends explicitly on the mesh dimensions. The unresolved SGS stress tensor $\overline{\tau_{ij}}^t$ is modelled using the Boussinesq assumption (Smagorinsky [1963]):

$$\overline{\tau_{ij}}^t - \frac{1}{3}\,\overline{\tau_{kk}}^t\,\delta_{ij} = -2\,\overline{\rho}\,\nu_t\,\widetilde{S}_{ij}\,, \tag{4}$$

$$\text{with}\;\; \widetilde{S}_{ij} = \frac{1}{2}\left(\frac{\partial \widetilde{u}_i}{\partial x_j} + \frac{\partial \widetilde{u}_j}{\partial x_i}\right) - \frac{1}{3}\,\frac{\partial \widetilde{u}_k}{\partial x_k}\,\delta_{ij}. \tag{5}$$

In Eq. (4), $\widetilde{S}_{ij}$ is the resolved strain rate tensor and ν_t is the SGS turbulent viscosity. The SGS energy flux $\overline{q_i}^t$ is modelled using a SGS turbulent heat conductivity obtained from ν_t by $\lambda_t = \overline{\rho}\,\nu_t\,/Pr_t$ where $Pr_t = 0.9$ is a constant turbulent Prandtl number. In the present case, this parameter has a very small effect on the wall heat fluxes since the boundary layers are fully resolved, so the turbulent contribution can be neglected in the viscous sub-layer provided that the SGS model has the appropriate behavior (close to walls, $\nu_t \approx 0$):

$$\overline{q_i}^t = -\lambda_t\,\frac{\partial \widetilde{T}}{\partial x_i}. \tag{6}$$

In Eq. (6), $\widetilde{T}$ is the Favre filtered temperature which satisfies the modified filtered state equation $\overline{p} = \overline{\rho}\,r\,\widetilde{T}$ (Moin et al. [1991], Ducros et al. [1996], Comte [1996]).

Flow solver and numerical parameters

The *elsA* software uses a cell centered approach on structured multiblock meshes. More information about this flow solver can be found in Cambier and Veuillot [2008]. For (steady-state) RANS

simulations, convective fluxes are computed with a second order centered scheme with classical artificial dissipation parameters k^2 and k^4 (Jameson et al. [1981]). Diffusive fluxes are computed with a second-order centered scheme. The pseudo time-marching is performed by using an efficient implicit time integration scheme, based on the backward Euler scheme and a scalar Lower-Upper (LU) Symmetric Successive Over-Relaxation (SSOR) method as proposed in Yoon and Jameson [1987]. The turbulent viscosity is computed with the two equations model of Smith [1995] based on a $k-l$ formulation and transition is detected with the criterion proposed by Abu-Ghannam and Shaw [1980].

For LES, convective fluxes are computed with a fourth order centered scheme, considering a minimal artificial dissipation (Ducros et al. [1999]). The time-marching scheme is based on a second order Dual Time Stepping method (Jameson [1991]). Such implicit algorithms are very attractive to reduce the simulation cost since the simulation is stable even with CFL numbers greater than 100. In the present case, 4,000 time steps are necessary to describe one through-flow time (the time for a particle dropped at the inlet to reach the outlet, *i.e.* $\approx 2.0ms$). It corresponds also to 60 time steps for one vortex shedding period. The subgrid scale model is the Wall-Adapting Local Eddy-Viscosity (WALE) model (Nicoud and Ducros [1999]), specially built to compute the turbulence effects in wall bounded flows (the value of ν_t vanishes at walls). Inside a mesh cell, local flow features are lost and only global quantities are represented by the SGS model.

Mesh grid

The flow domain is discretized with a multiblock approach, using an O-4H meshing strategy for the guide vane passage. A view of the computational domain is presented in Fig. 2(a) (for convenience the location of the probes used in the section "Discussion" is indicated on this figure). In order to limit the dependency of the solution to the inlet/outlet positions, the mesh extends up to 0.7 C uptream and 1.5 C dowstream the vane. The mesh represents 10% of the vane span (*i.e.* 10 mm in the spanwise direction)[1]. The minimum cell size is set to less than 2 μm all around the vane (corresponding to a mean wall distance y^+ of 1) with an expansion ratio near the wall close to 1.05. Typical grid dimensions are 651 points in the streamwise direction (781 points around the vane), 175 points in the pitchwise direction and 201 points in the spanwise direction. Experiments indicate that the mean flow is 2D. Indeed, the number of points in the spanwise direction is not a critical parameter for RANS and it can be reduced to only 5 points. Figure 2(b) presents the evolution of the normalized wall distance y^+ and the mesh spacings at walls $\Delta x^+ (= \Delta x/y^+)$, $\Delta z^+ (= \Delta z/y^+)$ around the vane. It shows that the maximum value of y^+ is always below 2. In other directions, mesh spacings are kept under acceptable values ($\overline{\Delta z^+} = 25$ and $\overline{\Delta x^+} = 150$). Based on this meshing strategy, the vane passage is represented with a 29.7×10^6 points grid (for LES) and a 0.7×10^6 points grid (for RANS).

Boundary conditions

An injection condition is applied at the inlet with parameters based on experimental data and a static pressure condition is applied downstream to set the outlet isentropic Mach number. An isothermal wall condition is applied at the vane walls with a uniform temperature and a condition of periodicity is used for lateral and radial ("top and bottom" of the domain) sections. A difficulty related to the studied flow is to take into account the desired inlet turbulence intensity. The solution used for RANS is to directly set the turbulence intensity for the transition criterion (the data is given by the user as an input). While sufficient for this application, the major drawback of this method is its lack of adaptability since the value of the turbulence intensity outside the boundary layer must be known (which is not always true). This problem is also an open question in the literature for LES. The choice in

[1] LES have been performed considering 5%, 10% and 20% of the experimental span. Results show that the mean wall heat transfer is identical for the configurations considering 10% and 20% of the experimental span.

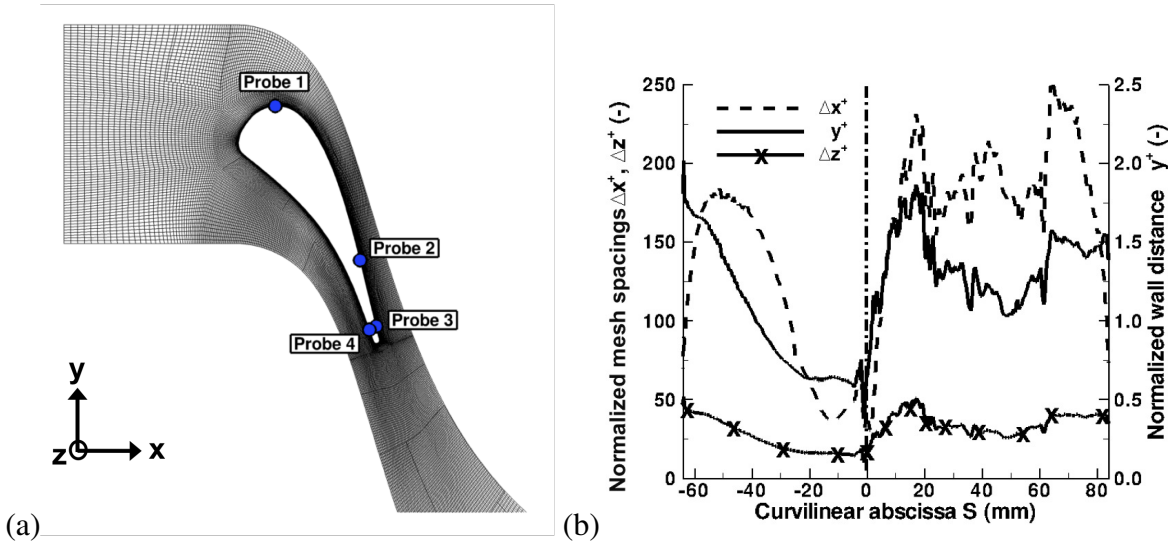

Figure 2: (a) Mesh grid with probe locations and (b) mesh spacings at wall Δx^+, y^+ and Δz^+ (LES)

the present case is not to directly inject turbulence (such as made by Bhaskaran and Lele [2010]) but it is rather to introduce perturbations in the flow that "mimic" the effects of turbulence. The method developed for LES is a simplified "2D" version of the "Synthetic Eddy Method" (SEM) proposed by Jarrin et al. [2006]. At the inlet, a set of independent random perturbations is superimposed to the mean velocity profil, such as:

$$u_i = \overline{u}_i + \Sigma u'_i \text{ with } \overline{u'_i} = 0. \tag{7}$$

Each perturbation u'_i is defined by its position (given by the random couple (y_i, z_i)) and its amplitude α (depending on a random wave number k_i), such that

$$u'_i = \alpha(k_i) e^{-\frac{1}{2}[|\frac{(y-y_i)}{L_i}|^2 + |\frac{(z-z_i)}{L_i}|^2]} \text{ with } \alpha(k_i) \sim k_i^4 e^{-k_i^2} \text{ and } L_i = 2\pi/k_i \tag{8}$$

At a given time t, the number of perturbations imposed at the domain inlet is $N_p = 2.A_{inlet}/{L_i}^2$ (with A_{inlet} the area of the inlet). Typically, for L_i=1mm the number of inlet perturbations is 1150. After a time $t_i = L_i/\overline{u_i}$, a new set of random perturbations is defined (new values for y_i, z_i, k_i). A condition $div\vec{u} = \vec{0}$ is also imposed at each grid point to reduce the "noise" induced by the perturbations. This synthetic eddy method requires a negligible computational time and the user can easily define the objective in terms of inlet turbulence intensity Tu_0 and most energetic length scale L_0. The generated synthetic turbulence is rather of good quality since after a distance $x = C/2$ (*i.e.* close to the vane leading edge), the turbulence intensity varies less than 20% with respect to the inlet value Tu_0.

RESULTS

All numerical simulations are performed on a SGI Altix computing platform. A RANS simulation needs only 20 CPU hours (with 2 computing cores) to reach convergence while the simulation of 10 through-flow times with LES requires 35,000 CPU hours (with 256 computing cores). Note also that 10 through-flow times is the time necessary to converge statistical quantities of the flow, but numerical data are then time-averaged on 5 other through-flow times before analysis.

Thanks to the experimental investigations led by Arts et al. [1990], most flow features have been identified in the studied configuration. Wall heat transfer is affected by the inlet turbulence intensity, turbulent to laminar transition, Mach and Reynolds numbers. An example of the observed flow

phenomena in the MUR235 test case ($Tu_0 = 6\%, Re_2 = 10^6$ and $M_{is,2} = 0.927$) is indicated in Fig. 3(a) (isentropic Mach number), Fig. 3(b) (wall friction coefficient C_{wf}) and Fig. 3(c) ($grad\rho/\rho$ flow field). The isentropic Mach number is plotted in Fig. 3(a) with respect to the curvilinear abscissa S ($S = 0$ corresponds to the vane leading edge, $S > 0$ is the suction side and $S < 0$ is the pressure side). A comparison of numerical data with experiments indicate that the simulation correctly reproduces experimental operating conditions. A normal shock is found on the suction side near the trailing edge, at the position $S = 60$ mm and a small plateau is observed in Fig. 3(a) on the suction side at $S = 20$ mm. In Fig. 3(b), the distribution of wall friction coefficient indicates that a transition of the suction side boundary layer occurs close to $S = 20$ mm (it corresponds to the small plateau observed on the isentropic Mach number distribution) while the pressure side boundary layer remains laminar. The influence of the shock on the wall friction coefficient is also well pointed out at $S = 60$ mm. In Fig. 3(c), the instantaneous $grad\rho/\rho$ flow field highlights flow phenomena such as the normal shock (1), the vortex shedding (2), the laminar to turbulent transition on the suction side (3) and the impact of large turbulent flow patterns on the pressure side (4). The instantaneous flow field shown in Fig. 3(c) also points out that the vortex shedding interacts with the normal shock about half a chord behind the trailing edge.

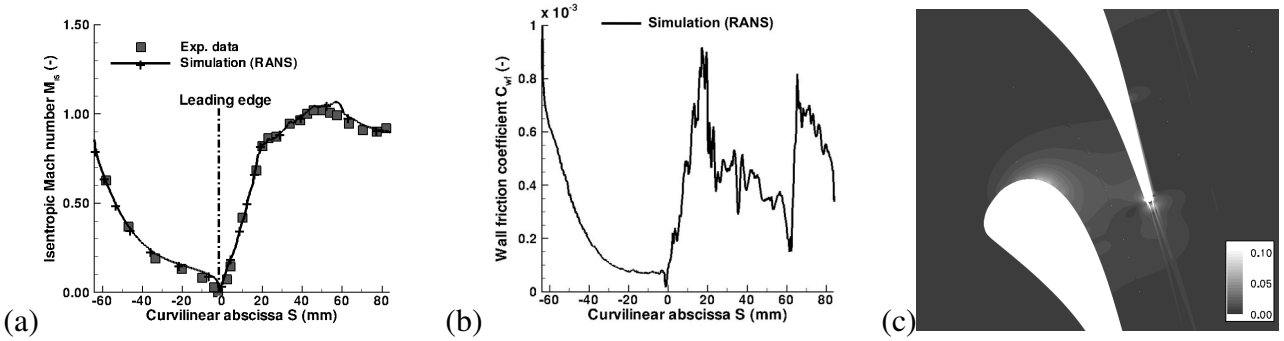

Figure 3: Distribution along the vane walls (MUR235): (a) isentropic Mach number and (b) wall friction coefficient C_{wf}. (c) Overview of the flow phenomena (instantaneous flow field computed with LES and colored with $grad\rho/\rho$)

MUR129 test case

The MUR129 test case ($Tu_0 = 1\%, Re_2 = 10^6$ and $M_{is,2} = 0.927$) is the simplest test case since the boundary layers remain mainly laminar on both suction and pressure sides. The heat transfer coefficient H is plotted on Fig. 4(a) (RANS) and Fig. 4(b) (LES). Both RANS and LES correctly estimate the wall heat fluxes on the pressure side and on most of the suction side. The heat transfer falls quickly after the leading edge, corresponding to the development of a laminar boundary layer both on pressure and suction sides. However, RANS and LES predict a boundary layer transition at $S = 62mm$ (corresponding roughly to the shock position) that is not seen on the experimental curve. This difference is related to the overestimation of the shock strength by the simulation with respect to experiments, as shown in Fig.3(a). The main difference between RANS and LES after transition is the level of the heat transfer coefficient ($H_{RANS} = 1100W/m^2.K$ and $H_{LES} = 600W/m^2.K$).

MUR235 test case

The MUR235 test case ($Tu_0 = 6\%, Re_2 = 10^6$ and $M_{is,2} = 0.927$) is much more complicated than the MUR129 test case, mainly due to the high inlet turbulence intensity. Results for the wall

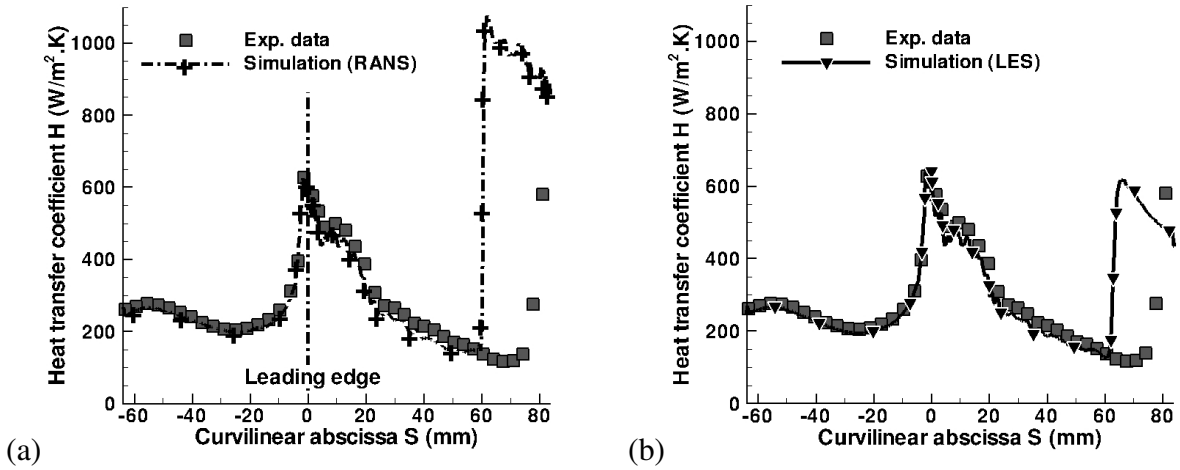

Figure 4: Heat transfer coefficient H predicted with (a) RANS and (b) LES (MUR129)

heat transfer are shown in Fig. 5(a) (RANS) and Fig. 5(b) (LES). The Reynolds number based on the momentum thickness Re_Θ and the pressure gradient along the vane curvilinear abscissa S are plotted in Fig. 6(a) (resp. Fig. 6(b)). To give a magnitude order, the theoretical laminar solution (Blasius theory[2]) for Re_Θ is also indicated in Fig. 6(a). Experiments show a "pre-transition" region from $S = 20mm$ (corresponding to the plateau on the isentropic Mach number curve in Fig. 3(a)) to $S = 60mm$. After transition ($S > 60mm$), the heat transfer on suction side is largely increased ($H \approx 800W/m^2.K$). Another effect of the high inlet turbulence intensity is to increase the heat flux on the pressure side wall by 50% with respect to the "purely" laminar boundary layer (MUR129 test case). The results presented in Fig. 5(a) indicate that the RANS simulation fails to accurately predict the wall heat transfer in this configuration. On the pressure side, the criterion does not detect any transition and the heat transfer coefficient H is identical to the MUR129 test case. As a consequence, the value of H is underestimated by 50%. The value of H near the leading edge is also underestimated by about 30%, highligthing the influence of inlet turbulent flow patterns. On the suction side, the RANS simulation finds the correct location for the onset of transition ($S \approx 20mm$) but it fails to estimate the transition length, leading to a strong overestimation of the heat transfer coefficient (at $S = 30mm$, the heat transfer is overestimated by 250%). After $S > 65mm$, the boundary layer is fully turbulent and RANS predicts the correct order of magnitude for the guide vane heating. These results are in agreement with other numerical works that consider RANS methods (Martelli et al. [2003]).

At these flow conditions, the contribution of LES is very interesting. First, the impact on the pressure side of inlet turbulent flow features is partially taken into account, as already shown by Bhaskaran and Lele [2010]. LES still underestimates the heat transfer on the pressure side, but the difference with experimental data is reduced to 20%. Then, the "pre-transition" region from $S = 20mm$ to $S = 60mm$ is correctly predicted with LES. On the suction side, the heat transfer coefficient is estimated with an error less than 5% (*i.e.* the experimental uncertainty) until $S = 65mm$. When the experimental boundary layer becomes fully turbulent (close to the trailing edge), the LES underestimates the wall heat transfer by 25%. As shown in Fig. 6(a) both RANS and LES predict the same transition point and both approaches predict a momentum thickness Θ smaller than the Blasius solu-

[2]The Blasius solution considers a laminar boundary layer without any pressure gradient ($\Theta_{Blasius} = 0.664 \times S \times Re_S^{-\frac{1}{2}}$).

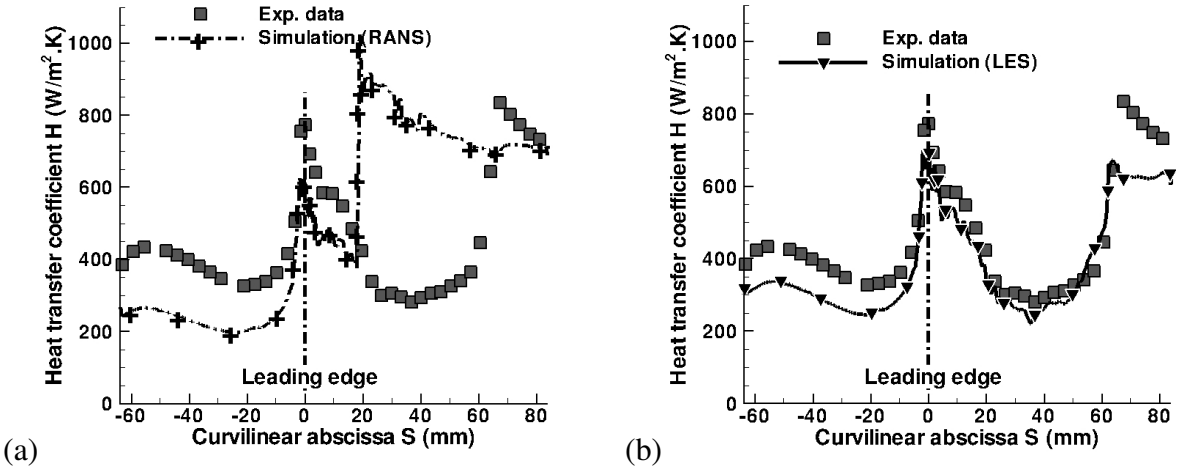

Figure 5: Heat transfer coefficient H predicted with (a) RANS and (b) LES (MUR235)

tion. As expected, the mean pressure gradient in the turbine vane is favorable. Thus it tends to push the flow towards the vane walls, reducing the momentum thickness. Finally, it is easy to correlate the transition point with the pressure gradient evolution (Fig. 6(b)). Both RANS and LES show that the local pressure gradient becomes negative on the suction side at $S = 15mm$ ($\approx 10,000$ Pa/mm), triggering transition. On the pressure side, the pressure gradient remains positive everywhere.

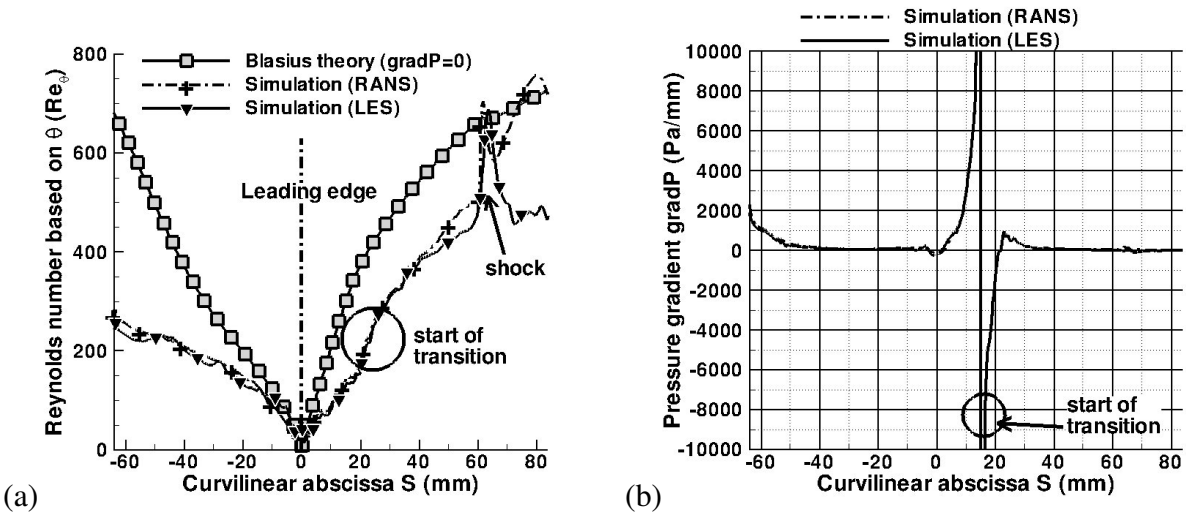

Figure 6: (a) Reynolds number based on the momentum thickness Θ and (b) pressure gradient at walls $\partial P/\partial S$ (MUR235)

MUR241 test case

The MUR241 test case ($Tu_0 = 6\%, Re_2 = 2.10^6$ and $M_{is,2} = 1.089$) is similar to the MUR235 test case in terms of flow phenomena, but operating flow conditions are closer to the flow conditions encountered in industrial configurations ($M_{is,2} > 1$ and oblique shock located at the vane trailing edge). Results for the wall heat transfer are shown in Fig. 7(a) (RANS) and Fig. 7(b) (LES). The

Reynolds number based on the momentum thickness Re_Θ and the pressure gradient along the vane curvilinear abscissa S are plotted in Fig. 8(a) (resp. Fig. 8(b)). Experiments indicate a fully turbulent boundary layer on the pressure side. The pre-transition region ($20 < S < 40mm$) on the suction side is reduced when compared to the MUR235 test case. The boundary layer is fully turbulent after $S = 40mm$ and the heat transfer on the suction side increases to $H = 720W/m^2.K$. The RANS simulation correctly estimates the value of H on the pressure side but close to the leading edge, the simulation still underestimates the heat transfer coefficient by 20%. On the suction side, the transition criterion detects the change of regime at $S = 15mm$ and the heat transfer coefficient is overestimated by 200% on most of the suction side (except in the trailing edge region). LES predicts the development of a laminar boundary layer on the pressure side and thus the heat transfer coefficient is largely underestimated (by about 50%). On the suction side, results are closer to experimental values (including at the vane leading edge), meaning LES is able to take into account the effect of the inlet turbulent flow patterns. The transition point is correctly predicted and the mean discrepancy with experiments on the suction side is less than 10%.

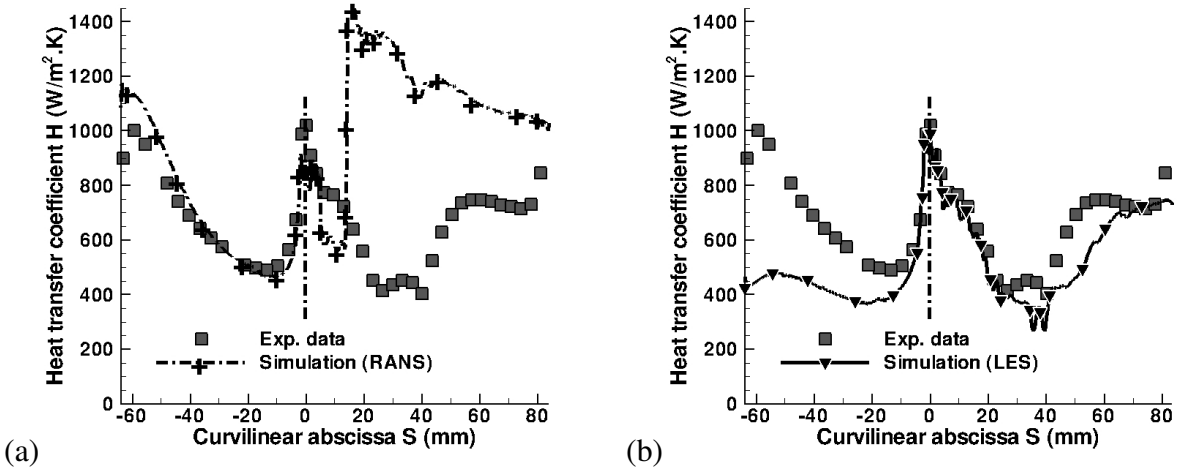

Figure 7: Heat transfer coefficient H predicted with (a) RANS and (b) LES (MUR241)

As shown in Fig. 8, RANS and LES do not predict the same transition point and the same evolution of the momentum thickness Θ (except on the pressure side). On the one hand, the RANS approach predicts a transition point on the suction side close to $S = 15mm$ (while experiments found it at $S = 20mm$). The reason is that the pressure gradient becomes negative at $S = 15$ mm. The momentum thickness (and thus Re_Θ) strongly increases from $S = 15mm$ ($Re_\Theta = 200$) to $S = 30mm$ ($Re_\Theta = 1000$). On the other hand, LES found the transition point at $S = 20mm$ and the peak of negative pressure gradient is predicts at $S = 25mm$. The Reynolds number based on the momentum thickness increases from $S = 20$ ($Re_\Theta = 200$) mm to the trailing edge ($Re_\Theta = 900$).

DISCUSSION

Previous results clearly underline that unsteady flows modify the development of boundary layers and thus the heat transfer coefficient. Based on the LES results, some of the unsteady flow features observed in the LS 89 guide vane are discussed in this section, with a particular interest for the boundary layer laminar to turbulent transition. Instantaneous flow field colored with the wall heat fluxes are presented in Fig. 9(a) (MUR129), Fig. 9(b) (MUR235) and Fig. 9(c) (MUR241).

For a low inlet turbulence intensity (MUR129, $Tu_0 = 1\%$), the boundary layer transition should

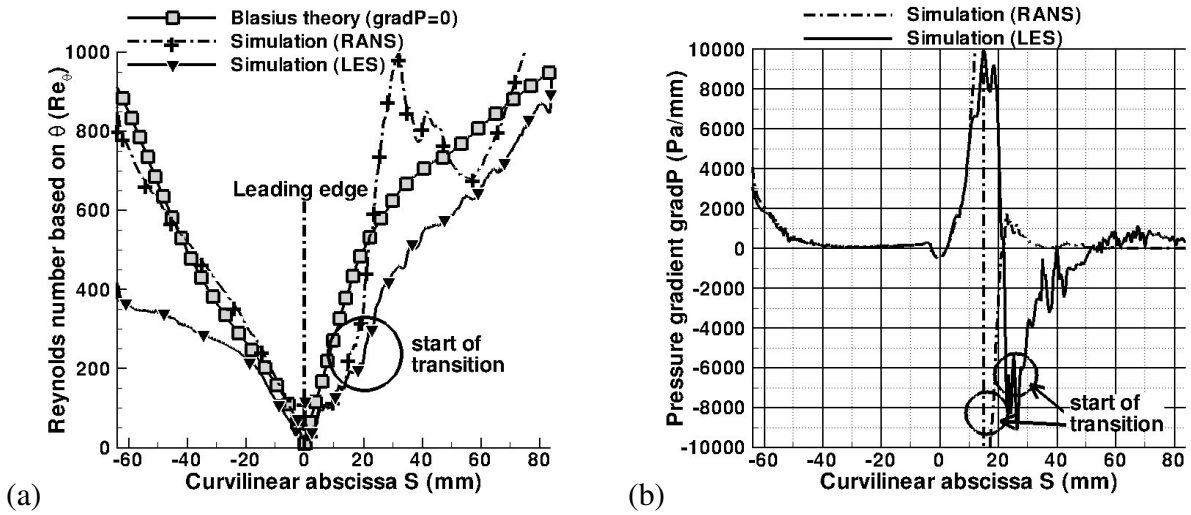

Figure 8: (a) Reynolds number based on the momentum thickness Θ and (b) pressure gradient at walls $\partial P/\partial S$ (MUR241)

be triggered by Tollmien-Schlichting waves (natural transition) but this is not what is observed in Fig. 9(a). The flow remains perfectly uniform in the spanwise direction only until $S = 40mm$. At this location, acoustic waves that are emitted at the vane trailing edge impact the vane suction side (see Fig.3(c)) and disturbances are observed in the radial direction. However these disturbances are damped and the transition is finally triggered by the interaction between the normal shock and the laminar boundary layer at $S = 62mm$.

At a higher turbulence intensity (MUR235, $Tu_0 = 6\%$), the transition proceeds more rapidly and the natural transition is by-passed (Simon and Kaszeta [2006]). The impact of turbulent flow patterns at the vane leading edge is well pointed out in Fig. 9(b). The development of long streaky flow features is also observed on the pressure side. This mechanism looks like Gortler vortices (Saric [1994]) and is responsible for a raise of the wall heat transfer (experiments show an increase by 80%). On the suction side, the boundary layer is laminar until $S = 20mm$. After this point, turbulent spots develop in the boundary layer ($2 < z < 4$) and the boundary layer becomes fully turbulent slightly before the shock at $S = 55mm$. The same phenomena are observed at higher Reynolds numbers (MUR241, $Tu_0 = 6\%$) with a higher intensity since the boundary layer on the suction side becomes turbulent at $S = 40mm$. On the pressure side, "Gortler" vortices largely increase the wall heat transfer but the LES does not see any transition of the boundary layer as observed in the experiments.

To complete the analysis of the MUR235 test case, a Power Spectrum Density is computed from an axial velocity signal $u(= \sqrt{u_x^2 + u_y^2})$, recorded in the boundary layer at $y^+ = 100$ and at different positions along the vane chord (see Fig. 2(a) for the probe locations). Each signal covers 1.5 through-flow times. The results are shown in Fig. 10 for the MUR235 test case. The first probe (Fig. 10(a)) is located on the suction side at $S = 15mm$, close to the first turbulent spots observed in the boundary layer. At this position, most energetic frequencies observed in the flow ($f < 10kHz$) are generated by the inlet perturbations (Eq. 7). This observation is coherent with the experimental data reported by Arts et al. [1990] (the set of registered inlet frequencies is $1kHz < f_{exp} < 10kHz$). As shown by the signal recorded by the probe 2, the development of the turbulent boundary layer is related to higher frequencies (Fig. 10(b)) and the flow energy is distributed along a wide range of frequencies ($f > 10kHz$). Close to the trailing edge on the suction side (probe 3), the flow unsteadiness is dominated by the vortex shedding frequency ($f_{VS} = 36kHz$). On the pressure side and close to

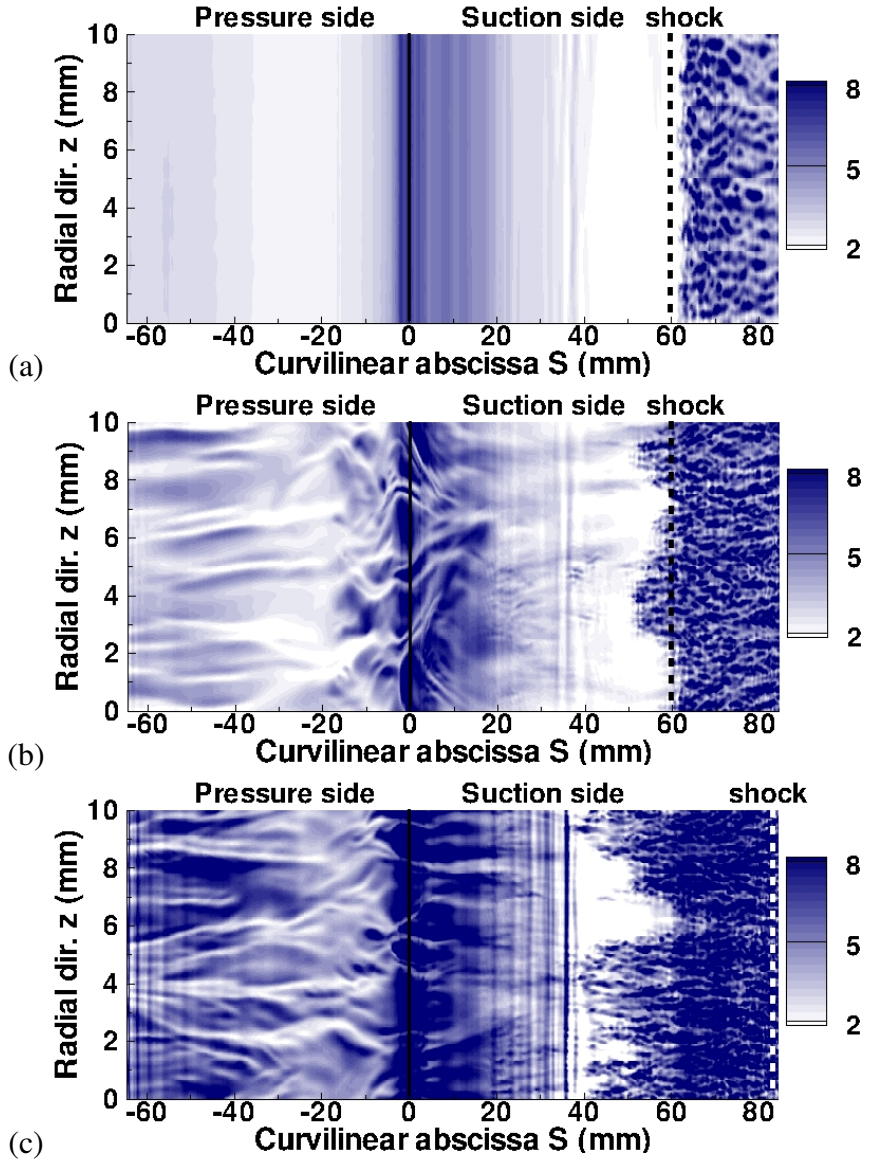

Figure 9: Instantaneous wall heat fluxes $Q(W/cm^2)$ computed with LES: (a) MUR129, (b) MUR235 and (c) MUR241

the trailing edge (probe 4), the effect of the vortex shedding is also observed but the most energetic frequencies are still low frequencies ($f < 10kHz$), that corroborate observations previously made about the laminar state of the boundary layer on the pressure side.

CONCLUSION

This paper relates the investigations made about the prediction of wall heat transfer in a highly loaded turbine guide vane (the so-called LS 89 vane). RANS and LES predictions have been compared to experimental data at different flow operating conditions ($M_{is,2} = 0.927/1.089$, $Re = 10^6/2.10^6$, $Tu_0 = 1/6\%$). Experiments and numerical simulations indicate that the wall heat transfer is very sensitive to the Reynolds number as well as to the inlet turbulence intensity. However, this second parameter is not easy to take into account both with RANS and LES methods. A simple method has been proposed to account for the inlet turbulence intensity with LES, based on a 2D formulation of the SEM method proposed by Jarrin et al. [2006] to perturb the inlet flow.

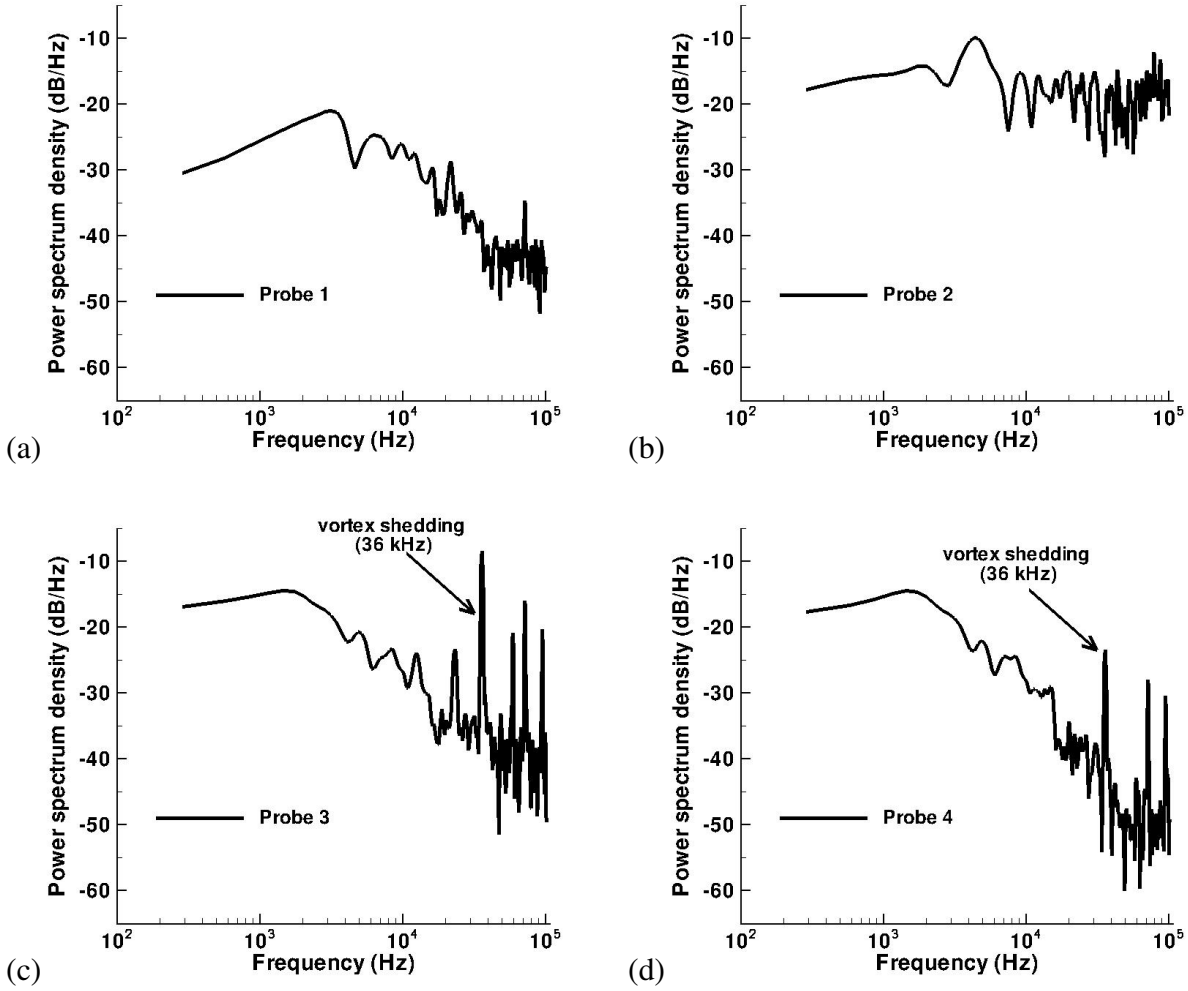

Figure 10: Power Spectrum Density computed from a velocity signal u (MUR235): (a) probe 1, (b) probe 2, (c) probe 3 and (d) probe 4 (see Fig. 2(a) for location). The transition on the suction side starts close to the probe 2 position.

On the one hand, the result analyses shows that the RANS approach (coupled with a transition criterion) is effective in predicting wall heat transfers when the boundary layer transition does not play a major role. Moreover this technique is efficient in terms of computational resources. However, the drawbacks of transition criteria are their lack of universality (*i.e.* a calibration is often necessary to obtain accurate predictions) and the difficulty to use them in an industrial context. The adoption of transport equations for the quantities handled by transition criteria could (at least partially) overcome this problem (Menter et al. [2004], Smirnov and Smirnovsky [2009]). This recent approach could help in the prediction of transition in complex geometries, based on the transport of specific quantities (such as Re_Θ). However, in the case of a laminar boundary layer and even with such an approach, a RANS simulation fails to accurately estimate the contribution of the turbulent structures to the wall heat transfer (Smirnov and Smirnovsky [2009]). The use of a RANS approach is thus better adapted to cooled nozzle guide vanes where the transition usually occurs close to the leading edge (due to cooling holes).

On the other hand, LES is a very promising method, especially when an accurate description of the boundary layer transition is necessary (configurations without cooling devices at the leading edge).

While LES still requires a very large computational power (a 30M points grid is necessary to represent only 10% of the vane span), this method is able to describe natural and by-passed transitions as well as the transition triggered by the shock-boundary layer interaction. The main interest for LES is its capability to describe unsteady flows in a wide range of industrial applications (transition, vortex shedding, etc.). Finally, this paper demonstrates that LES is ready to help in the understanding of complex flow phenomena that are observed in high-pressure turbines (including at high Reynolds numbers). However, an effort is still necessary to use LES in an industrial context (full 3D, stage configurations, etc.) and modelling could be improved.

ACKNOWLEDGEMENTS

Many thanks to Tony Arts (VKI) for his help in this study. The work presented in this paper has also largely benefited from CERFACS supercomputers and GENCI-CINES computing facilities (under the project fac 6074). These supports are greatly acknowledged. The authors also thank people of the CERFACS CFD team for helpful discussions.

REFERENCES

B.J. Abu-Ghannam and R. Shaw. Natural transition of boundary layers - the effects of turbulence, pressure gradient, and flow history. *J. of Mechanical Engineering Science*, 22(5):213–228, 1980.

T. Arts, M. Lambert de Rouvroit, and A. W. Rutherford. Aero-thermal investigation of a highly loaded transonic linear turbine guide vane cascade. Technical Note 174, Von Karman Institute, 1990.

R. Bhaskaran and S. K. Lele. Large eddy simulation of free stream turbulence effects on heat transfer to a high-pressure turbine cascade. *J. of Turbulence*, 11(6), 2010.

R. J. Boyle and A. A. Ameri. Grid orthogonality effects on turbine midspan heat transfer and performance. *J. Turbomachinery*, 119(1):31–38, 1997.

L. Cambier and J. P. Veuillot. Status of the elsa cfd software for flow simulation and multidisciplinary applications. In *46th AIAA Aerospace Science Meeting and Exhibit*, number 664, 2008.

P. Comte. New tools in turbulence modelling. vortices in incompressible les and non-trivial geometries. Springer-Verlag, France, 1996. Course of Ecole de Physique des Houches.

H. Consigny and B.E. Richards. Short duration measurements of heat transfer rate to a gas turbine rotor blade. *J. of Engineering for Power*, 104:542–551, 1982.

F. Duchaine, S. Mendez, F. Nicoud, A. Corpron, V. Moureau, and T. Poinsot. Coupling heat transfer solvers and large eddy simulations for combustion applications. *Int. J. of Heat and Fluid Flow*, 30: 1129–1141, 2009.

F. Ducros, P. Comte, and M. Lesieur. Large-eddy simulation of transition to turbulence in a boundary layer developing spatially over a flat plate. *J. Fluid Mech.* , 326:1–36, 1996.

F. Ducros, V. Ferrand, F. Nicoud, C. Weber, D. Darrack, and T. Poinsot. Large-eddy simulation of the shock/turbulence interaction. *J. Computational Physics*, 152:517–549, 1999.

A. Gehrer and H. Jericha. External heat transfer predictions in a highly loaded transonic linear turbine guide vane cascade using an upwind based navier-stokes solver. *J. Turbomachinery*, 121(3):525–531, 1999.

J. C. Han, S. Dutta, and S. V. Ekkad. *Gas Turbine Heat Transfer and Cooling Technology*. Taylor & Francis, New York, NY, USA, 2001.

A. Jameson. Time dependent calculations using multigrid, with applications to unsteady flows past airfoils and wings. In *AIAA Computational Fluid Dynamics Conference*, 1991.

A. Jameson, W. Schmidt, and E. Turkel. Numerical solution of the euler equations by finite volume methods using runge-kutta time stepping schemes. In *AIAA 14th Fluid and Plasma Dynamics Conference*, 1981.

N. Jarrin, S. Benhamadouche, D. Laurence, and R. Prosser. A synthetic eddy method for generating inflow conditions for large eddy simulations. *Int. J. of Heat and Fluid Flow*, 27(585-593), 2006.

M. W. Johnson. A bypass transition model for boundary layers. *J. Turbomachinery*, 116(4):759–764, 1994.

Y. Liu. Aerodynamics and heat transfer predictions in a highly loaded turbine blade. *Int. J. of Heat and Fluid Flow*, 28:932–937, 2007.

F. Martelli, P. Adami, and E. Belardini. Heat transfer modelling in gas turbine stage. Technical Report ADA419187, University of Florence, 2003.

R. E. Mayle. The role of laminar-turbulent transition in gas turbine engines. *J. Turbomach.*, 113: 509–537, October 1991.

F. R. Menter, R. B. Langtry, S. R. Likki, Y. B. Suzen, P. G. Huang, and S. Volker. A correlation based transition model using local variables. part 1: model formulation. In *ASME Turbo Expo*, number GT2004-53452. Vienna, Austria, 2004.

P. Moin, K. D. Squires, W. Cabot, and S. Lee. A dynamic subgrid-scale model for compressible turbulence and scalar transport. *Phys. Fluids* , A 3(11):2746–2757, 1991. doi: 10.1063/1.858164.

F. Nicoud and F. Ducros. Subgrid-scale stress modelling based on the square of the velocity gradient. *Flow, Turb. and Combustion* , 62(3):183–200, 1999. doi: 10.1023/A:1009995426001.

T. Poinsot and D. Veynante. *Theoretical and Numerical Combustion*. R.T. Edwards, 2nd edition., 2005.

S. B. Pope. *Turbulent flows*. Cambridge University Press, 2000.

P. Sagaut. *Large Eddy Simulation for incompressible flows*. Scientific computation series. Springer-Verlag, 2000.

W. S. Saric. Gortler vortices. *Annu. Rev. Fluid Mech.*, 26, 1994.

D. L. Schultz and T. V. Jones. Heat transfer measurements in short duration hypersonic facilities. Report 165, AGARD, 1973.

T. W. Simon and R. W. Kaszeta. Transition to turbulence under low-pressure turbine conditions. *Annals of the New York Academy of Sciences*, 934:37–51, 2006.

J. Smagorinsky. General circulation experiments with the primitive equations: 1. the basic experiment. *Mon. Weather Rev.* , 91:99–164, 1963.

E. Smirnov and A. Smirnovsky. Turbine vane cascade heat transfer predictions using a modified version of the $\gamma - Re_{\theta t}$ laminar-turbulent transition model. In *Int. Symp. On Heat Transfer in Gas Turbine Systems*, 2009.

B. R. Smith. Prediction of hypersonic shock wave turbulent boundary layer interactions with the k-l two equaton turbulence model. In *AIAA 33rd Aerospace Sciences Meeting and Exhibit*, 1995.

S. Yoon and A. Jameson. An LU-SSOR scheme for the euler and navier-stokes equations. In *AIAA 25th Aerospace Sciences Meeting*, 1987.

B. Zhong and P. G. Tucker. LES and hybrid LES/RANS simulations for conjugate heat transfer over a matrix of cubes. In *43rd AIAA Aerospace Sciences Meeting and Exhibit*, 2005.